High-Valent Oxo, Methoxorhenium Complexes: Models for Intermediates and Transition States in Proton-Coupled Multi-Electron Transfer Reactions

M. S. Ram, Lisa M. Skeens-Jones, Christopher S. Johnson, Xiao Lian Zhang, Charlotte Stern, Dong I. Yoon, Donald Selmarten, and Joseph T. Hupp*

Contribution from the Department of Chemistry, Northwestern University, Evanston, Illinois 60208

Received August 9, 1993[⊗]

Abstract: *trans*-Dioxorhenium(V) tetrapyridyl species are currently under active investigation as model systems for interfacial two-electron, two-proton transfer reaction sequences (Jones-Skeens et al. *Inorg. Chem.* **1992**, *31*, 3879). We now find that the corresponding oxo, methoxo complexes can be prepared from the dioxo species and methyl trifluoromethanesulfonate. The new complexes behave nearly identically with the analogous oxo, hydroxo complexes—with one important exception: CH_3^+, unlike H^+, does not dissociate from the oxo ligand. As a direct consequence, the usually elusive rhenium oxidation state IV is stabilized with respect to redox disproportionation and is observable for several complexes at high pH. The ability to detect this state, in turn leads to (1) direct access to the formal reduction potentials for the isolated $1e^-$ redox couples comprising the overall two-electron transfer (key information for understanding multi-electron transfer kinetics), (2) elucidation of the profound structural and energetic consequences of the initial protonation (methylation) step in the dioxorhenium(V) reduction kinetics, (3) estimates for pK_a of $(O)(HO)Re^{VI}L_4^{3+}$ (exceptionally negative), and (4) estimates for the first pK_a of $(HO)_2Re^{III}L_4^+$ (extremely large and positive). The combination of (1) and (2), in principle, provides sufficient information to characterize completely the energetic accessibility of key intermediate species lying just before or just after the transition state for the two-electron, two-proton reduction of dioxorhenium(V) at electrochemical interfaces.

Introduction

High-valent metal−oxo and −dioxo complexes often display an ability to accept multiple electrons as well as protons in a chemically reversible fashion at a single well-defined energy or potential,[1−7] e.g.:[8]

$$t\text{-}(O)_2Re^{V}(L)_4^+ + 2e^- + 2H^+ \xrightarrow{E_f} t\text{-}(HO)_2Re^{III}L_4^+ \quad (1)$$

The propensity toward multi-electron transfer (multi-ET) has motivated a number of attempts to exploit the class of systems in catalytic or redox−catalytic reaction sequences,[9] including water oxidation,[10] alkene epoxidation,[11] selective alcohol → ketone transformations,[12] etc.

In part, because of their low formal reduction potentials (E_f), the dioxorhenium(V) complexes shown specifically in eq 1 are *not* exceptionally useful as redox catalysts.[13] On the other hand, we have found them to be remarkably versatile model reactants for systematic studies of interfacial (i.e., electrochemical) multi-ET kinetics—an issue of obvious importance in redox-mediated catalysis, but also of more general significance.[14] Our preliminary experimental studies of reaction 1 (where L = pyridine (py) or any of several py derivatives) reveal that (a) the kinetics

[⊗] Abstract published in *Advance ACS Abstracts,* January 15, 1995.

(1) Representative studies involving ruthenium: (a) Adeyemi, A. S.; Dovletoglou, A.; Gaudalupe, A. R.; Meyer, T. J. *Inorg. Chem.* **1992**, *31*, 1375. (b) Marmion, M. E.; Takeuchi, K. J. *J. Am. Chem. Soc.* **1988**, *110*, 1472. (c) Che, C. M.; Tang, W. T.; Wong, W. T.; Lai, T. F. *J. Am. Chem. Soc.* **1989**, *111*, 9048. (d) Blaho, J. K.; Goldsby, K. A. *J. Am. Chem. Soc.* **1990**, *112*, 6132.

(2) Representative studies involving osmium: (a) Pipes, D. W.; Meyer, T. J. *Inorg. Chem.* **1986**, *25*, 4042. (b) Takeuchi, K. J.; Thompson, M. S.; Pipes, D. W.; Meyer, T. J. *Inorg. Chem.* **1984**, *23*, 1845. (c) Dobson, J. C.; Takeuchi, K. J.; Pipes, D. W.; Geselowitz, D. A.; Meyer, T. J. *Inorg. Chem.* **1986**, *25*, 2357.

(3) Representative studies involving manganese: (a) Thorp, H. H.; Sarneski, J. E.; Brudvig, G. W.; Crabtree, R. H. *J. Am. Chem. Soc.* **1989**, *111*, 9249. (b) Chan, M. K.; Armstrong, W. H. *J. Am. Chem. Soc.* **1989**, *111*, 9121. (c) Bradbury, J. R.; Schultz, F. A. *Inorg. Chem.* **1986**, *25*, 4408.

(4) Studies involving rhenium: (a) Pipes, D. W.; Meyer, T. J. *Inorg. Chem.* **1986**, *25*, 3256. (b) Ram, M. S.; Johnson, C. S.; Blackbourn, R. L.; Hupp, J. T. *Inorg. Chem.* **1990**, *29*, 238. (c) Ram, M. S.; Jones, L. M.; Ward, H. J.; Wong, Y.-H.; Johnson, C. S.; Subramanian, P.; Hupp, J. T. *Inorg. Chem.* **1991**, *30*, 2928. Jones-Skeens, L. M.; Zhang, X. L.; Hupp, J. T. *Inorg. Chem.* **1992**, *31*, 3879.

(5) Related studies involving dioxorhenium: (a) Winkler, J. R.; Gray, H. B. *J. Am. Chem. Soc.* **1983**, *105*, 1373. (b) Winkler, J. R.; Gray, H. B. *Inorg. Chem.* **1985**, *24*, 346. (c) Brewer, J. C.; Gray, H. B. *Inorg. Chem.* **1989**, *28*, 3334. (d) Thorp, H. H.; Kumar, C. V.; Turro, N. J.; Gray, H. B. *J. Am. Chem. Soc.* **1989**, *111*, 4364. (e) Newsham, M. D.; Giannelis, E. P.; Pinnavia, T. J.; Nocera, D. G. *J. Am. Chem. Soc.* **1988**, *110*, 3885. (f) Brewer, J. C.; Gray, H. B. *Reprints: Symposium on Selective Catalytic Oxidation of Hydrocarbons*, ACS Division of Petroleum Chemistry, American Chemical Society: Washington, D.C., 1990; pp 187−191. (g) Johnson, C. S.; Mottley, C.; Hupp, J. T.; Donzer, G. I. *Inorg. Chem.* **1992**, *31*, 5143.

(6) For recent discussions, see: (a) Thorp, H. H. *J. Chem. Educ.* **1992**, *69*, 250. (b) Thorp, H. H. *Chemtracts: Inorg. Chem.* **1991**, *3*, 171.

(7) For reviews of metal−oxo chemistry; see: (a) Holm, R. H. *Chem. Rev.* **1987**, *87*, 1401. (b) Nugent, W. A.; Mayer, J. M. *Metal-Ligand Multiple Bond*; John Wiley: New York, 1988.

(8) The doubly protonated Re(III) species could alternatively be represented as an aquo−oxo species.

(9) For a somewhat dated but excellent review, see: Meyer, T. J. *J. Electrochem. Soc.* **1984**, *131*, 221c.

(10) Representative reports: (a) Gilbert, J. A.; Eggleston, D. S.; Murphy, W. R.; Geselowitz, D. A.; Gersten, S. W.; Hodgson, D. W.; Meyer, T. J. *J. Am. Chem. Soc.* **1985**, *107*, 3855. (b) Hurst, J. K.; Zhou, J.; Lei, Y. *Inorg. Chem.* **1992**, *31*, 1010.

(11) Representative reports: (a) Dobson, J. C.; Seok, W. K.; Meyer, T. J. *Inorg. Chem.* **1986**, *25*, 1514. (b) Che, C. M.; Wong, K. Y.; Mak, T. C. *J. Chem. Soc., Chem. Commun.* **1985**, 988. (c) Groves, J. T.; Ahn, K. H. *Inorg. Chem.* **1987**, *26*, 381.

(12) Representative reports: (a) Thompson, M. S.; Meyer, T. J. *J. Am. Chem. Soc.* **1982**, *104*, 4106. (b) McHatton, R. C.; Anson, F. C. **1984**, *23*, 3955.

(13) For examples, however, of dioxorhenium-based electrocatalysis, see: Thorp, H. H.; Van Houten, J.; Gray, H. B. *Inorg. Chem.* **1989**, *28*, 889 and ref 4a.

0002-7863/95/1517-1411$09.00/0

of interfacial e^- and coupled H^+ transfer, in contrast to the thermodynamics, necessarily involve sequential, stepwise transfer (see Scheme 1); (b) rapid, uphill protonation precedes the initial reduction step; and (c) depending on the exact circumstances, either the first (Re(V→IV)) or second (Re(IV→III)) redox step can be rate controlling.[15]

Scheme 1

$$t\text{-}(O)_2Re^{V}L_4^{+} + H^+ \rightarrow t\text{-}(O)(HO)Re^{V}L_4^{2+} \quad (2)$$

$$t\text{-}(O)(HO)Re^{V}L_4^{2+} + e^-(\text{electrode}) \rightarrow t\text{-}(HO)(O)Re^{IV}L_4^{+} \quad (3)$$

$$t\text{-}(O)(HO)Re^{IV}L_4^{+} + e^-(\text{electrode}) \rightarrow t\text{-}(HO)(O)Re^{III}L_4^{0} \quad (4)$$

$$t\text{-}(O)(HO)Re^{III}L_4^{0} + H^+ \rightarrow t\text{-}(HO)_2Re^{III}L_4^{+} \quad (5)$$

Thus, the singly protonated form of Re^{IV} can be regarded as the species lying either just after or just before the two-electron, two-proton transfer reaction transition state.[16]

Obviously, considerable mechanistic insight could be derived if this "near transition state" species could be isolated and characterized. Unfortunately, Re^{IV} is unstable toward disproportionation (eq 6) at all accessible pH's:[4a,d]

$$2t\text{-}(O)(HO)Re^{IV}L_4^{+} \rightarrow t\text{-}(O)_2Re^{V}L_4^{+} + t\text{-}(HO)_2Re^{III}L_4^{+} \quad (6)$$

We wish to report here, however, the synthesis and characterization of a family of rhenium complexes which display, at high pH's, the elusive oxidation state IV. The new compounds are oxo, methoxo analogues of the dioxorhenium species. Remarkably, the methyl group behaves like a nonlabile proton, providing, in effect, spectroscopic and electrochemical access to the key intermediate species $t\text{-}(O)(HO)Re^{V}L_4^{2+}$ and $t\text{-}(O)(HO)Re^{IV}L_4^{+}$. This, in turn, leads to (1) direct access to the formal potentials (E_f) for the isolated $1e^-$ redox couples comprising the overall two-electron transfer,[17] (2) elucidation of the profound structural and energetic consequences of the initial protonation step in Scheme 1, (3) estimates for the pK_a of $(O)(HO)Re^{VI}L_4^{3+}$ (exceptionally negative), and (4) estimates for the first pK_a of $(HO)_2Re^{III}L_4^{+}$ (extremely large and positive). Besides its obvious relevance to multi-ET kinetics, item 2 is also clearly pertinent to current studies of photoinitiated proton transfer, and especially back H^+ transfer,[18,19] e.g.:

$$t\text{-}(O)_2ReL_4^{+} \xrightarrow{h\nu} t\text{-}(O)_2ReL_4^{+*} \xrightarrow{H^+}$$

$$t\text{-}(O)(HO)ReL_4^{2+*} \rightarrow t\text{-}(O)(HO)ReL_4^{2+} \rightarrow t\text{-}(O)_2ReL_4^{+} + H^+ \quad (7)$$

Items 3 and 4, on the other hand, are perhaps most significant in the context of possible mechanisms for *trans*-dioxorhenium-based oxidative[13] and reductive[4a] electrocatalytic reactions, respectively.

Experimental Section

Materials. Tetrabutylammonium hexafluorophosphate ($TBAPF_6$) was prepared from HPF_6 and the corresponding bromide salt, and purified by recrystallization (3×). Ammonium hexafluorophosphate (95%) was purchased from Aldrich and used as received. Reagent grade CH_2Cl_2 was dried over alumina. All other starting materials were reagent grade chemicals from Aldrich or Mallinckrodt and were used without further purification. Aqueous solutions were prepared by using water from a Milli-Q purification system.

Metals Complexes. The new compounds were derived in each case from related *trans*-$(O)_2ReL_4^{+}$ species, whose syntheses have already been described.[20] Abbreviations for L: dmap = 4-dimethylaminopyridine, pyrrpy = 4-pyrrolidinopyridine, MeOpy = 4-methoxypyridine, Me_2py = 3,4-dimethylpyridine (3,4-lutidine), Me-py = 4-methylpyridine, and py = pyridine.

***trans*-[(O)(MeO)Re(dmap)$_4$](PF$_6$)$_2$.** $[(O)_2Re(dmap)_4]Cl$ (1.2 g) was dissolved in 100 mL of dry CH_2Cl_2. Methyl trifluoromethanesulfonate (10 g) was added and the solution was stirred at room temperature for 30 min. As the reaction proceeded, the color turned from yellow to purple and the solution became homogenous. Rotary evaporation of solvent at 35 °C gave an oil which was then dissolved in 10 mL of methanol. Addition of 10 mL of saturated NH_4PF_6 solution, followed by 200 mL of ether caused precipitation. The crude product was collected on a glass frit and washed with 2 × 30 mL of toluene and 3 × 40 mL of ether/ethanol. The compound was purified by doubly chromatographing on alumina with 98:2 CH_2Cl_2/2-propanol, and isolated by addition of ether: yield (multiple syntheses), 20−60%; ^1H NMR (acetone-d_6) δ 7.80 (d, J = 7.50 Hz, pyH α to N, 8 H), 6.88 (d, J = 7.50 Hz, pyH β to N, 8 H), 3.92 (s, OCH_3, 3 H), 3.28 (s, $N(CH_3)_2$, 24 H); ^{13}C NMR (acetone-d_6) δ 157.12 (pyC γ to N), 151.86 (pyC α to N), 109.58 (pyC β to N), 59.10 (OCH_3), 39.34 ($N(CH_3)_2$). Anal. Calcd for $C_{29}F_{12}H_{43}N_8O_2P_2Re$: C, 34.4; H, 4.25; N, 11.0; F, 22.8; P, 6.21. Found: C, 34.6; H, 4.27; N, 10.63; F, 22.8; P, 6.16.

***trans*-[(O)(MeO)Re(MeOpy)$_4$](PF$_6$)$_2$.** This complex was prepared in a similar fashion, except with $[(O)_2Re(MeOpy)_4]Cl$ as a starting material. The complex was purified by twice passing a CH_2Cl_2 solution through a silica gel column initially prepared with CH_2Cl_2. Acetone, however, was used as the eluent. Addition of ether immediately precipitated the light purple product: yield (multiple syntheses), 15−53%; ^1H NMR (acetone-d_6) δ 8.40 (d, pyH α to N, 8 H), 7.39 (d, pyH β to N, 8 H), 4.14 (s, $ReOCH_3$ and $pyOCH_3$, 15 H). Anal. Calcd for $C_{25}F_{12}H_{31}N_4O_6P_2Re$: C, 31.29; H, 3.25; N, 5.83. Found: C, 31.29; H, 3.21; N, 5.80.

***trans*-[(O)(MeO)Re(py)$_2$(dmap)$_2$](PF$_6$)$_2$.** $[(O)_2Re(py)_2(dmap)_2]Cl$ was dissolved in 100 mL of dry CH_2Cl_2 and reacted with 10 g of methyl trifluoromethanesulfonate. The yellow/brown reaction mixture was stirred for 1 h. $TBAPF_6$ (1 g) was added to the resulting red/purple solution. The crude product was precipitated by addition of 200 mL of ether and then washed twice with toluene and twice with an ether/ethanol mixture. The compound was purified by twice passing a CH_2Cl_2 solution through a silica gel column, eluting with 90:10 CH_2Cl/2-propanol. Addition of ether precipitated a bright purple product: yield (multiple syntheses), 7−50%; ^1H NMR (acetone-d_6) δ 8.58 (d, J = 5.22 Hz, pyH α to N, 4 H), 8.26 (t, J = 7.77 Hz, pyH γ to N, 2 H), 7.93 (t, J = 6.93 Hz, pyH β to N, 4 H), 7.86 (d, J = 7.30, dmapH) α to N, 4 H), 6.82 (d, J = 7.30 Hz, dmapH β to N, 4 H), 4.08 (s, OCH_3, 3 H), 3.24 (s, $N(CH_3)_2$, 12 H); ^{13}C NMR (acetone-d_6) δ 157.15 (dmapC γ to N), 151.66 (dmapC α to N), 144.19 (pyC γ to N), 128.31 (pyC β to N), 109.80 (dmapC β to N), 59.39 (OCH_3), 39.3 ($N(CH_3)_2$). Anal.

(14) For related discussions of multi-ET kinetics see, for example: (a) Pfennig, B. W.; Bocarsly, A. B. *Commun. Inorg. Chem.* **1992**, *13*, 261. (b) Richardson, D. E.; Taube, H. *Coord. Chem. Rev.* **1984**, *60*, 107. (c) Ram, M. S.; Hupp, J. T. *J. Phys. Chem.* **1990**, *94*, 2378.

(15) A mechanistic discrepancy between cyclic voltammetry and steady-state microelectrode findings was noted in ref 4d, and tentatively ascribed to differences in reaction medium and pH and to other effects. We have since found, via extensive digital simulation studies, that the critical variable is the overpotential region (i.e., thermodynamic driving force region) in which the rate measurements are made. At the formal potential, reaction 4 is rate determining; at somewhat more negative potentials, the rate is controlled by reaction 3.

(16) Skeens-Jones, L. M. Ph.D. Dissertation, Northwestern University, 1992.

(17) "Direct" to the extent that the oxo−hydroxo/oxo−methoxo analogy is valid.

(18) Liu, W.; Welch, T. W.; Thorp, H. H. *Inorg. Chem.* **1992**, *31*, 4044.

(19) Lu, H.; Skeens-Jones, L. M.; Hupp, J. T. Unpublished results.

(20) (a) Brewer, J. C.; Gray, H. B. *Inorg. Chem.* **1989**, *28*, 3344. (b) Ram, M. S.; Hupp, J. T. *Inorg. Chem.* **1991**, *30*, 130.

Calcd for $C_{25}F_{12}H_{33}N_6O_2P_2Re$: C, 32.43; H, 3.59; N, 9.07. Found: C, 32.11; H, 3.64; N, 8.90.

***trans*-[(O)(MeO)Re(pyrrpy)$_4$](PF$_6$)$_2$.** This compound was prepared and isolated in an analogous fashion to [(O)(OMe)Re(py)$_2$(dmap)$_2$]-(PF$_6$)$_2$, except that [(O)$_2$Re(pyrrpy)$_4$](PF$_6$) was used as a starting material. The complex was purified by doubly chromatographing on alumina with 95:5 CH_2Cl_2/ethanol. The dark purple product precipitated upon addition of ether: yield (multiple syntheses), 65−75%; ^{1}H NMR ($CDCl_3$) δ 7.53 (d, J = 7.06 Hz, pyH α to N, 8 H), 6.53 (d, J = 7.06 Hz, pyH β to N, 8 H), 3.68 (s, OCH_3, 3 H), 3.56−3.51 (m, aliphatic H α to N, 16 H), 2.08−2.03 (m, aliphatic H β to N, 16 H); ^{13}C NMR ($CDCl_3$) δ 153.35 (pyC γ to N), 150.57 (pyC α to N), 109.49 (pyC β to N), 58.17 (OCH_3), 47.55 (aliphatic C α to N), 25.19 (aliphatic C β to N). Anal. Calcd for $C_{37}F_{12}H_{51}N_8O_2P_2Re$: C, 39.82; H, 4.61; N, 10.04. Found (two determinations, same sample): C, 40.20, 40.18; H, 4.48, 4.40; N, 9.82, 9.82.

***trans*-[(O)(MeO)Re(Me$_2$-py)$_4$](PF$_6$)$_2$.** [(O)$_2$Re(Me$_2$-py)$_4$]Cl (2.2 g) was dissolved in 80 mL of dry CH_2Cl_2, and 4 g of methyl trifluoromethanesulfonate was added to the solution. The reaction mixture was stirred for 2 h, the solution slowly becoming more purple in color. $TBAPF_6$ (1 g) was added, followed by 200 mL of ether, to yield an oil. The oil was redissolved in acetone, then precipitated as a solid after addition of 300 mL of ether. The crude product was washed twice each with toluene, chloroform, and ether. The complex was purified by doubly chromatographing on silica with acetone as the eluent. The light pink/purple product was precipitated upon addition of ether: yield (multiple syntheses), 8−28%; ^{1}H NMR (acetone-d_6) δ 8.40 (s, py H α to N, 4 H), 8.33 (d, py H α' to N, 4 H), 7.67 (d, py H β to N, 4 H), 4.31 (s, OCH_3, 3 H), 2.70 (s, $pyCH_3$, 12 H), 2.23 (s, $pyCH_3$, 12 H). Anal. Calcd for $C_{29}F_{12}H_{39}N_4O_2P_2Re$: C, 36.59; H, 4.13; N, 5.88. Found: C, 36.20; H, 4.09; N, 5.64.

***trans*-[(O)(MeO)Re(Me$_2$py)$_4$](CF$_3$SO$_3$)$_2$.** The preparation and purification of this complex were analogous to those described for the PF_6^- salt, but without the addition of $TBAPF_6$. Anal. Calcd for $C_{31}F_6H_{39}N_4O_8ReS_2$: C, 38.79; H, 4.09; N, 5.84. Found: C, 37.49; H, 3.80; N, 5.62. (Note that although the analysis for carbon is less than ideal (it is satisfactory for the PF_6^- salt), the structure of the compound has been established by X-ray crystallography (see below).)

trans-[(O)(MeO)Re(Me-py)$_4$](PF$_6$)$_2$. The preparation of this complex was analogous to the preparation of [(O)(OMe)Re(Me$_2$-py)$_4$](PF$_6$)$_2$, except that [(O)$_2$Re(Me-py)$_4$]Cl was treated with 4 g of methyl trifluoromethanesulfonate. The complex was purified by chromatographing on silica with 95:5 CH_2Cl_2/ethanol as eluent. Addition of ether immediately precipitated the pale pink/purple product: yield (multiple syntheses), 0−10%; ^{1}H NMR (acetone-d_6) δ 8.52 (d, py H α to N, 8 H), 7.77 (d, py H β to N, 8 H), 4.27 (s, OCH_3, 3 H), 2.79 (s, $pyCH_3$, 12 H). Anal. Calcd for $C_{25}F_{12}H_{31}N_4O_2P_2Re$: C, 33.52; H, 3.49; N, 6.26. Found (two determinations, same sample): C, 32.00, 31.77; H, 3.25, 3.36; N, 5.97, 5.93. Low yields and general difficulty in preparing this compound (several attempts failed completely) prevented us from obtaining sufficient material to pursue further purification (by additional chromatography). Nevertheless, the presumably slightly impure compound exhibited electrochemical and spectral properties (including satisfactory ^{1}H NMR) fully consistent with those expected for an authentic member of the (O)(MeO)ReL$_4^{2+}$ series. Despite the doubtful analysis for carbon, therefore, we believe that the isolated material is primarily the desired oxo, methoxo complex.

Measurements. UV−visible absorption spectra were obtained with a Cary 14 spectrophotometer that had been rebuilt by OLIS. Infrared spectra were obtained from KBr pellets by using a Mattson FTIR instrument. Raman spectra were initially obtained via continuous excitation at 457.9 and 514.5 nm with either a Spectra Physics Series 2000 or an Ion Laser Technologies argon ion laser, as previously described.[5g] Additional measurements at 647.1 nm were made with a Spectra Physics Series 2000 Kr^+ source. Later measurements were made with a Spex Triplemate spectrometer and CCD detector by using either a Coherent Inova 400 argon ion laser (514.5 nm) or a Tsunami/Spectra Physics titanium/sapphire laser (725, 751−755 nm; pumped by the Coherent Inova 400) as the excitation source. (The Tsunami source is mode locked at 86 MHz, but was employed as a pseudo-CW source.) Samples were dissolved in 50:50 acetonitrile/water, placed in a spinning NMR tube, and configured in either a 180° backscattering geometry or a 90° geometry.

Table 1. Summary of Crystal Structure Data for [(O)(MeO)Re(Me$_2$py)$_4$](CF$_3$SO$_3$)$_2$·CH$_3$COCH$_3$

formula	$ReS_2O_9F_6N_4C_{34}H_{45}$
M	1018.07
cryst size, mm	0.490 × 0.082 × 0.042
cryst system	monoclinic
space group	$P2_1/c$ (No. 14)
a, Å	15.256 (2)
b, Å	20.604 (3)
c, Å	12.976 (4)
β, deg	90.41 (2)
V, Å^3	4079 (3)
Z	4
d_{calcd}, g cm^{-3}	1.658
μ(Mo Kα), cm^{-1}	31.96
radiation	graphite-monochromated Mo Kα (λ = 0.71069 Å)
scan type	$\omega-\theta$
2θ range, deg	4−47
scan width, deg	(1.00 + 0.35 tan θ)
unique data	6231
unique date with $I > 3\sigma(I)$	3365
no. of parameters	461
$R(F)$	0.047
$R_w(F)$	0.049
GOF	1.50

Formal potentials were estimated by cyclic voltammetry by using a standard three-electrode configuration and instrumentation previously described.[4c] Working electrodes were generally glassy carbon disks (3-mm diameter Tokai GC-205, or 1-mm diameter electrodes from Cypress Systems). All potentials are referenced to a saturated (NaCl) aqueous calomel electrode (ssce). Mixed solvents (50:50 CH_3CN/water) were a necessity in most electrochemical experiments because of solubility problems in purely aqueous solutions. Conductivity and pH control were maintained with buffers at μ = 0.1 M or at the pH extremes with strong acid or bases, as outlined previously.[4c] Apparent pH's (designated pH*) were determined with a Beckman 31 pH meter and a Beckman Model 39386 combination electrode (or calculated as −log [H$^+$] for pH*'s below 1.0).

X-ray Crystallography. Crystals of *t*-[(O)(MeO)Re(Me$_2$py)$_4$](CF$_3$SO$_3$)$_2$ suitable for X-ray crystallographic measurements were grown from slow diffusion of an acetone/ether solution. A pale purple, transparent, columnar crystal having the dimensions 0.490 × 0.082 × 0.042 mm was mounted on a glass fiber using oil (Paraton-N, Exxon). Measurements were made on an Enraf Nonius CAD4 diffractometer with graphite monochromated Mo Kα radiation. Cell constants and an orientation matrix were obtained from a least-squares refinement using the setting angles of 25 centered reflections in the range 18.1 < 2θ < 20.7°. Based on the systematic absences of $h0l$ ($l \neq 2n$) and $0k0$ ($k \neq 2n$), the space group was umambiguously determined to be $P2_1/c$ (#14). The data were collected using the $\omega-\theta$ scan technique to a maximum 2θ value of 47°. Of the 8228 reflections which were collected, 6231 were unique. The intensities of three standard reflections, which were measured after every 90 min of X-ray exposure time, remained constant throughout data collection, indicating crystal and electronic stability (no decay correction was applied). The linear absorption coefficient for Mo Kα is 32.0 cm^{-1}. An analytical absorption correction was applied which resulted in transmission factors from 0.76 to 0.87. A summary of the crystal structure is given in Table 1.

The structure was solved using heavy atom methods (Patterson and Fourier techniques) and refined by full-matrix least-squares refinement based on 3365 absorption corrected reflections with $I > 3\sigma(I)$ and 461 variable parameters. The nonhydrogen atoms were refined either anisotropically or isotropically to give final $R(F)$ = 0.047 and $R_w(F)$ = 0.049. TEXSAN 4.0 crystallographic software was used throughout the calculations.[21]

(21) The TEXRAY Structure Analysis Program Packagem Molecular Structure Corporation, College Station, TX, 1986.

A pyridine ring of one of the lutidine ligands and a $CF_3SO_3^-$ anion were found to be disordered. In the pyridine ring the atoms N31 and C32A were not disordered and were in full population. The populations of the other disordered carbon atoms were 0.605 for C33A–C36A and 0.395 for C32B–C35B (C36B is C32A). The thermal parameters of the disordered carbon atoms were independently refined isotropically. The fluorine populations of the $CF_3SO_3^-$ anion were 0.638 for F11A–F13A and 0.362 for F11B–F13B, and the oxygen populations were 0.441 for O11A–O13A and 0.559 for O11B–O13B. Group thermal parameters were isotropically refined for the fluorines and the oxygens. Tables of crystal data, positional parameters, thermal parameters, interatomic distances, bond angles, and structure factors are available as supplementary material.

Results

Synthesis. Our initial efforts to add CH_3^+ to dioxorhenium complexes emphasized CH_3I as the methylating agent. These efforts were completely unsuccessful. Also unsuccessful were subsequent attempts with an even more potent methylating agent, $CF_3SO_3CH_3$—at least when the methylation targets were *trans*-$(O)_2Re(py)_4^+$, *trans*-$(O)_2Re(py\text{-}x)_4^+$ (where x is an electron-withdrawing substituent), or any of several *cis*-dioxorhenium-(V) complexes. We ultimately were successful, however, with *trans*-dioxorhenium targets featuring comparatively electron-rich pyridyl ligands such as 3,4-dimethylpyridine and 4-dimethylaminopyridine.

Since three of the six precursor complexes (dioxorhenium species) contain tertiary amines as ligand substituents, it is important to consider the possibility that methylation alternatively or additionally occurs at nitrogen. That this is *not* the case is shown most clearly by (1) elemental analysis—particularly fluorine analysis, which would be much higher if additional methyl cations (and, therefore, additional hexafluorophosphate anions) were present; (2) ^1H and ^{13}C NMR spectra which are fully consistent with the oxo, methoxo formulations (see assignments), but inconsistent with further methylation at nitrogen, and (3) X-ray crystallography (see below) which shows specifically for $[(O)(MeO)Re(py)_2(dmap)_2](PF_6)_2$ that amine methylation has not occurred. (Other less direct arguments, based on anticipated substituent effects upon electrochemical potentials and electronic absorption spectra, similarly point toward a lack of reactivity at the pendent amine sites.)

Returning to the observed oxo methylation, we found within the reactive subset of rhenium species that the extent of reactivity (i.e., the oxo, methoxo product yield) progressively increased with increasing (cumulative) py ligand substituent electron-donating strength (Me-py < Me_2py < MeOpy < dmap ≈ pyrrpy). Nevertheless, even with the constraint that electron-rich pyridine ligands be used, a total of six new complexes proved accessible via the methyltriflate route:

$$t\text{-}(O)_2ReL_4^+ + CF_3SO_3CH_3 \rightarrow t\text{-}(O)(MeO)ReL_4^{2+} + CF_3SO_3^- \quad (8)$$

Crystallography. Definitive assignment of the new complexes as oxo, methoxo complexes was achieved by X-ray crystallography. The crystallographic studies, however, were not without their difficulties. Several compounds yielded crystals which diffracted, but whose structures could not be fully refined. One of the partially refined structures was for $[t\text{-}(O)(MeO)Re(py)_2(dmap)_2](PF_6)_2$. Here the extent of refinement was sufficient, however, to establish that (1) the dmap ligands are coordinated trans to each other, (2) CH_3 has added to one of the two available oxo ligands, and (3) methyl cations have not added to the amine substituents. Further details are given in the supplementary material.

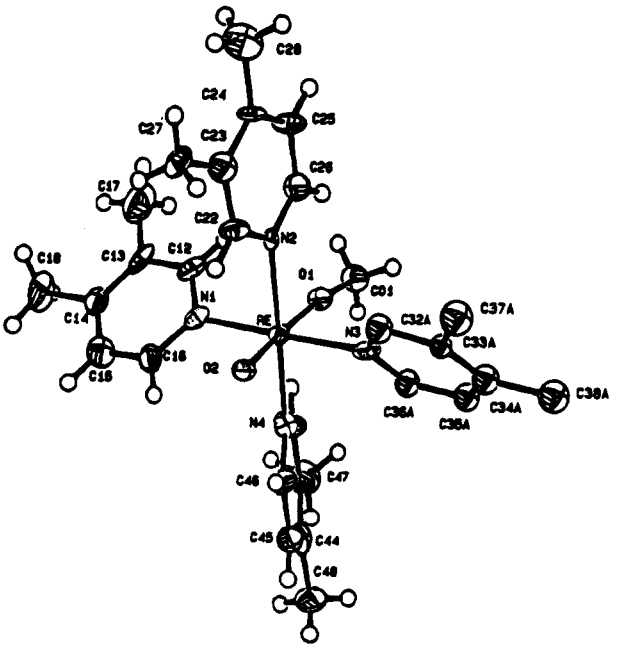

Figure 1. ORTEP drawing of $t\text{-}(O)(MeO)Re(Me_2py)_4^{2+}$.

Table 2. Selected Bond Distances (Å) and Angles (deg) for $[(O)(MeO)Re(Me_2py)_4](CF_3SO_3)_2$

Re–O1	1.829(7)	O1–Re–N4	88.3(3)
Re–O2	1.693(7)	O2–Re–N1	92.7(4)
Re–N1	2.131(8)	O2–Re–N2	90.9(3)
Re–N2	2.146(8)	O2–Re–N3	90.2(4)
Re–N3	2.138(9)	O2–Re–N4	90.3(3)
Re–N4	2.136(9)	N1–Re–N2	89.4(3)
O1–CO1	1.44(1)	N1–Re–N3	176.8(4)
O1–Re–O2	177.6(3)	N1–Re–N4	88.1(3)
Re–O1–CO1	172.1(7)	N2–Re–N3	92.0(3)
O1–Re–N1	89.3(3)	N2–Re–N4	177.2(3)
O1–Re–N2	90.5(3)	N3–Re–N4	90.5(3)
O1–Re–N3	87.8(4)		

A complete structure was ultimately obtained for $[t\text{-}(O)(MeO)Re(Me_2py)_4](CF_3SO_3)_2$. An ORTEP drawing is shown in Figure 1. Selected bond distances and bond angles are listed in Table 2. Notable features in comparison in dioxo complexes include (1) elongation of the methylated oxygen–rhenium bond to 1.83 Å (from ca. 1.77 Å), (2) compression of the nonmethylated oxygen–rhenium bond to 1.69 Å, and (3) constancy of the nitrogen–rhenium bond lengths (at ca. 2.14 Å). If one accepts 1.77 Å as a typical rhenium–oxygen double-bond length[23] and 2.04 Å (i.e., the sum of covalent radii) as a reasonable single-bond length, then the structure suggests multiple bonding to both oxo ligands (bond orders of, say, 1.5 and 2.5, respectively). The Re–N bond lengths, on the other hand, are consistent with single-bond formation. One other structural feature of note is the nearly linear rhenium–oxygen–carbon configuration. On the basis of several literature precedents, we had expected an angle of ca. 120° to 145° for Re–O1–C1.[24] In any case, the more linear configuration here would be consistent again with rhenium–oxygen multiple bonding.

Electronic Absorption Spectra. Shown in Figure 2 are representative UV–visible absorption spectra for (O)(MeO)-

(22) (a) Johnson, J. W.; Brody, J. F.; Ansell, G. B.; Zentz, S. *Inorg. Chem.* **1984**, *23*, 2415. (b) Lock, C. J. L.; Turner, G. *Acta Crystallogr.* **1978**, *B34*, 923. (c) Lock, C. J. L.; Turner, G. *Can. J. Chem.* **1977**, *55*, 333. (d) Calvo, C.; Krishnamacher, N.; Lock, C. J. L. *J. Cryst. Mol. Struct.* **1971**, *1*, 161.

(23) Cotton, F. A.; Lippard, S. J. *Inorg. Chem.* **1965**, *4*, 1621.

Table 3. Electronic Absorption Spectral Data for Oxo–Methoxo, Oxo–Hydroxo, and Dioxo Rhenium(V) Complexes

complex	λ_{max}, nm (ϵ, M^{-1} cm^{-1})		
$(O)(MeO)Re(pyrrpy)_4^{2+}$	265 (3.9×10^4)	314 (6.5×10^4)	569 (1.7×10^3)
$(O)(HO)Re(pyrrpy)_4^{2+}$ [a]	267 (5.2×10^4)	315 (5.2×10^4)	574 (1.7×10^3)
$(O)_2Re(pyrrpy)_4^{+}$	273 (5.2×10^4)	353 (4.2×10^4)	465 (2.6×10^3)
$(O)(MeO)Re(dmpa)_4^{2+}$	262 (3.3×10^4)	313 (5.7×10^4)	565 (1.7×10^3)
$(O)(HO)Re(dmap)_4^{2+}$ [b]	261 (2.4×10^4)	315 (5.1×10^4)	568 (1.3×10^3)
$(O)_2Re(dmap)_4^{+}$	272 (4.7×10^4)	358 (3.7×10^4)	462 (2.3×10^3)
$(O)(MeO)Re(py)_2(dmap)_2^{2+}$		295 (3.4×10^4)	531 (1.5×10^3)
$(O)(HO)Re(py)_2(dmap)_2^{2+}$		305 (4.6×10^4)	533 (1.7×10^3)
$(O)_2Re(py)_2(dmap)_2^{+}$	253 (1.7×10^4)	363 (1.0×10^4)	471 (1.6×10^3)
$(O)(MeO)Re(MeOpy)_4^{2+}$		271 (2.9×10^4)	521 (9.0×10^2)
$(O)(HO)Re(MeOpy)_4^{2+}$ [c]		276 (2.9×10^4)	521 (9.0×10^2)
$(O)_2Re(MeOpy)_4^{+}$	281 (7.0×10^3)	347 (2.7×10^4)	438 (1.5×10^3)
$(O)(MeO)Re(Me_2py)_4^{2+}$		281 (1.7×10^4)	511 (7.0×10^2)
$(O)(HO)Re(Me_2py)_4^{2+}$		284 (1.2×10^4)	510 (6.4×10^2)
$(O)_2Re(Me_2py)_4^{+}$	275 (5.7×10^3)	356 (2.9×10^4)	416 (2.1×10^3)
$(O)(MeO)Re(Mepy)_4^{2+}$		280 (1.5×10^4)	508 (7.2×10^2)
$(O)_2Re(Mepy)_4^{+}$	247 (1.6×10^4)	353 (3.2×10^4)	429 (2.0×10^3)

[a] Solvent is 50:50 CH_3CN/H_2O. [b] 0.5 M H_2SO_4 (50:50 CH_3CN/H_2O0. Higher acid concentrations led to decomposition. [c] 2.0 M H_2SO_4 (50:50 CH_3CN/H_2O).

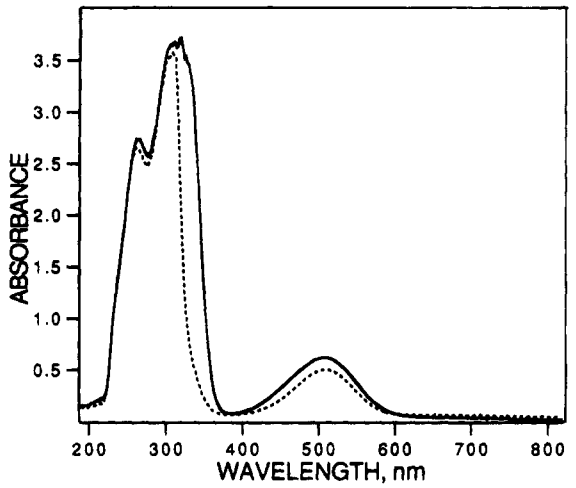

Figure 2. UV–visible spectra for *t*-$(O)(MeO)Re(Me_2py)_4^{2+}$ (solid line) and *t*-$(O)(HO)Re(Me_2py)_4^{2+}$ (dashed line) in 50:50 CH_3CN/H_2O with 2 M H_2SO_4.

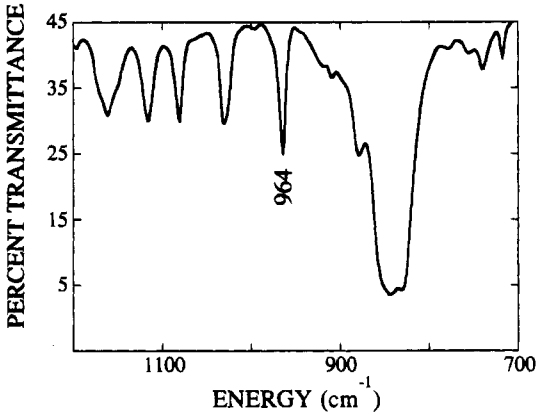

Figure 3. Infrared absorption spectrum for [*t*-$(O)(MeO)Re(Me_2py)_4$]-$(PF_6)_2$ (KBr pellet).

ReL_4^{2+} and $(O)(HO)ReL_4^{2+}$. The similarities are striking, especially in comparison to the spectroscopy for the parent dioxo complex. On the basis of its low extinction coefficient, the broad feature near 530 nm in the $(O)(MeO)ReL_4^{2+}$ spectrum is assigned as a d–d (or ligand-field) transition. (The corresponding feature in the dioxorhenium spectrum appears at 430 nm.) Note that the d–d transition is formally forbidden; evidently it borrows significant intensity from neighboring allowed transitions.[26] The oxo, methoxo complexes also exhibit an intense absorption anywhere between 280 and 315 nm. Assignment as metal-to-ligand (pyridine) charge transfer (MLCT) is made on the basis of (a) the appearance of an apparently related MLCT transition near 350 nm in the corresponding dioxo complexes (i.e., 400 to 900 meV lower in energy), coupled with (i.e., correlated with) (b) a 650- to 1100-mV increase in the Re(VI/V) potential following methylation. Finally, for some complexes a third feature near 260 nm can be resolved. Almost certainly this feature is a pyridine ligand centered transition.

Table 3 shows that the electronic absorption spectrum displays a substantial pyridyl ligand dependence. Both the MLCT and d–d transitions shift toward higher energy as the ligand basicity[27] decreases. (In contrast, in the parent dioxo complexes only the d–d transition responds to ligand basicity variations.)[5d,f] Perhaps the most striking feature of Table 3, however, is the very close parallel between $(O)(MeO)ReL_4^{2+}$ and $(O)(HO)ReL_4^{2+}$ spectra, both in terms of intensities and energetics. Clearly the electronic consequences of oxo ligand methylation are very well approximated by protonation. Finally, we note that none of the oxo, methoxo complexes is detectably luminescent, even when irradiated in nonhydroxylic solvents, again reminiscent of oxo, hydroxo species.[18]

Vibrational Spectroscopy. A representative infrared absorption spectrum ($[(O)(MeO)Re(Me_2py)_4](PF_6)_2$; KBr pellet) is shown in Figure 3. The single most intense feature is a broad absorption near 830 cm^{-1} that is associated with the hexafluorophosphate counterion. Also seen are several intense peaks

(24) (a) Bakir, M.; Paulson, S.; Goodson, P.; Sullivan, B. P. *Inorg. Chem.* **1992**, *31*, 1129. (b) Forsellini, E.; Casellato, U.; Graziani, R.; Carletti, M. C.; Magon, L. *Acta Crystallogr.* **1984**, *C40*, 1795. (c) Ciani, G. F.; D'Alfonso, G.; Romitiz, P. F. l Sironi, A.; Freni, M. *Inorg. Chim. Acta* **1983**, *72*, 29. (d) Haymore, B. L.; Goeden, G. V. *Inorg. Chem.* **1983**, *22*, 157.

(25) (a) Paradis, J. A.; Wertz, D. W.; Thorp, H. H. *J. Am. Chem. Soc.* **1993**, *115*, 5308. (b) Ballhausen, C. J.; Gray, H. B. *Inorg. Chem.* **1962**, *1*, 111. (c) Hopkins, M. D.; Miskowski, V. M.; Gray, H. B. *J. Am. Chem. Soc.* **1986**, *108*, 6908.

(26) From Table III we observe that the extinction coefficient for the d–d absorption increases (as expected) as the MLCT/d–d energy gap decreases.

(27) Sawada, M.; Ichihara, M.; Yukawa, Y.; Nakachi, T.; Tsumo, Y. *Bull. Chem. Soc. Jpn.* **1980**, *53*, 2055.

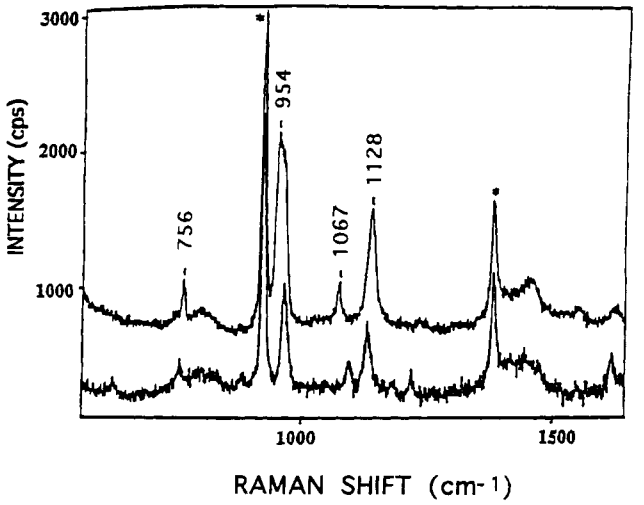

Figure 4. Resonance Raman spectra (514.5-nm excitation) of *t*-(O)(MeO)Re(dmap)$_4^{2+}$ (top) and *t*-(O)(MeO)Re(Me$_2$py)$_4^{2+}$ (bottom) in 50:50 CH_3CN/water. Asterisks denote solvent peaks. (The complex counterion in both instances was PF_6^-.)

between 1000 and 1200 cm^{-1}. Those at 1050 and 1161 cm^{-1} are probably pyridyl ligand based. The peak at 1117 cm^{-1}, on the other hand, is tentatively ascribed to an O−CH_3 stretch. The increase peak at 964 cm^{-1} is assigned as the rhenium−oxo stretch. Evidently missing (as one would expect) is the asymmetric O=Re=O stretch at 822 cm^{-1} (although conceivably the absorption could be obscured by the feature associated with PF_6^-). In principle, more definitive assignments could be made (particularly for vibrations at 966 and 1117 cm^{-1}) by examining isotopically substituted compounds. Unfortunately, these efforts were frustrated by the anticipated lack of reactivity of CD_3I toward *t*-(O)$_2$ReL$_4^+$ and by the commercial unavailability of ^{18}O-labeled water when the synthetic work was carried out.

As an alternative to IR, several resonance Raman experiments were performed. Because Raman is both a vibrational *and* an electronic spectroscopic method, it offers a means for identifying selected vibrations more rigorously. In particular, the existence of resonance enhancement effects permits one to distinguish solvent, counterion, and other spurious vibrations from those associated with the molecular chromophore (in this case, (O)(MeO)ReL$_4^{2+}$). At a more detailed level, it permits specific assignments to be made with very high confidence when the nature of the corresponding resonant electronic transition is known (since, to a first approximation, only vibrations directly coupled to that transition will be enhanced in the scattering spectrum).

Figure 4 shows resonance Raman scattering spectra (514.5-nm excitation for a representative pair of oxo, methoxo complexes. Once solvent modes (marked by asterisks) are excluded, fairly simple vibrational spectra emerge; peaks are seen at roughly 751−756, 954−961, 1060−67, and 1120−1124 cm^{-1}. (Table 4 summarizes data for five complexes.) As expected, resonance enhanced scattering by these modes is most intense for the most strongly absorbing complexes. (More direct evidence for resonance enhancement at 514.5 nm comes from off-resonance measurements with 647.1, 725, 751, 753, and/or 755 nm excitation (not shown).)

Vibrational assignments are most easily made by considering the corresponding electronic absorption spectra (Figure 2, Table 3). Excitation at 514.5 nm is resonant with a transition that promotes an electron from d_{xy} to d_{xz} and/or d_{yz} (i.e., a transition that increases electron density along the oxo−rhenium−methoxo axis or core). We have previously shown[5g] with the analogous *dioxo* species that d−d excitation induces resonant scattering from vibrations involving the core, but *not* (with minor exceptions) from vibrations associated with pyridyl ligands (effectively orthogonal to the core). On this basis, the intense peak at 954 (961) cm^{-1} (~964 cm^{-1} in Figure 3) can now be assigned with some confidence as the expected rhenium−oxo stretch, where the increase in frequency in comparison to the symmetrical O=Re=O stretch (902−908 cm^{-1}; notably absent here) is suggestive of rhenium−oxygen triple bond formation. Other prominent bands at 743 and 1124 cm^{-1} (both d−d enhanced) are tentatively assigned (as above) as Re−OMe and C−O(methoxy) stretches. The remaining feature at 1060−1067 cm^{-1} also exhibits enhancement in spectra for *trans*-(O)$_2$ReL$_4^+$ (d−d excitation).[5g] Previous H/D labeling studies with *t*-(O)$_2$Re(py)$_4^+$ clearly indicated that the vibration is associated with pyridine (an in-plane C−H(D) deformation appearing at ca. 1072−1075 cm^{-1} (slightly different instrument calibration)).[5g] Support for a similar assignment here is provided by measurements made on (O)(MeO)Re(dmap)$_4^{2+}$ with 354-nm excitation (resonant with metal-to-pyridine charge transfer, see Table 3). Under these conditions the mode near 1067 cm^{-1} is strongly enhanced, as are several new modes which are clearly associated with the derivatized pyridine ligand. (As with the O=Re=O stretch in (O)$_2$ReL$_4^+$,[5g] modes assigned as Re−OCH_3 and Re=O in the oxo, methoxo complex also exhibit UV enhancement. The relative extent of UV versus visible enhancement, however, is considerably greater for the vibration at 1067 cm^{-1}.)

Table 4. Resonance Raman Data (514.5-nm Excitation) for (O)(MeO) ReL$_4^{2+}$ Complexes

	vibrational assignment,[b] cm^{-1}			
complex[a]	Re−OCH_3	Re≡O	i.p. C−H def (py)	ReO−CH_3
(O)(MeO)Re(pyrrpy)$_4^{2+}$	743	954	1060	1124
(O)(MeO)Re(dmap)$_4^{2+}$	756	954	1067	1128
(O)(MeO)Re(py)$_2$(dmap)$_2^{2+}$	754	960	1065	1122
(O)(MeO)Re(MeOpy)$_4^{2+}$	751	965	*c*	1125
(O)(MeO)Re(Me$_2$py)$_4^{2+}$	751	961	*c*	1120

[a] Counterion in each case is PF_6^-. The solvent is 50:50 CH_3CN/H_2O. [b] See text for explanation of assignments. Vibrational frequencies are referenced to the Q"(C−C) mode of CH_3CN (981 cm^{-1}) as an internal standard. [c] Scattering not detected.

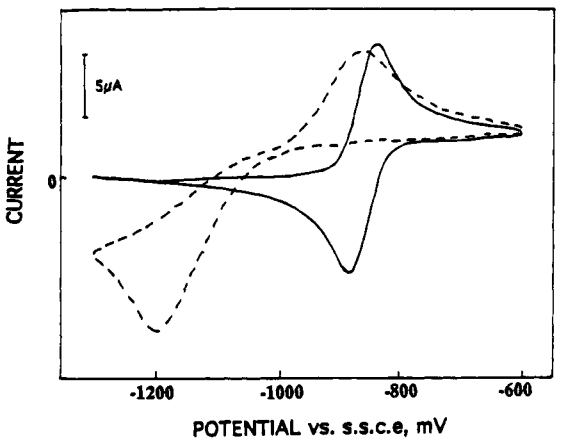

Figure 5. Background-subtracted cyclic voltammograms (sweep rate = 100 mV/s) for the reduction and re-oxidation of *t*-(O)(MeO)Re(dmap)$_4^{2+}$ (solid line) and *t*-(O)$_2$Re(dmap)$_4^+$ dashed line in 50:50 CH_3CN/water at pH* = 8.0.

Aqueous Electrochemistry. Shown in Figure 5 are representative background-subtracted cyclic voltammograms for the 2e$^-$ reductions of *t*-(O)$_2$Re(dmap)$_4^+$ (eq 1) and *t*-(O)(MeO)Re(dmap)$_4^{2+}$ (eq 9). Two observations, in particular, are worth

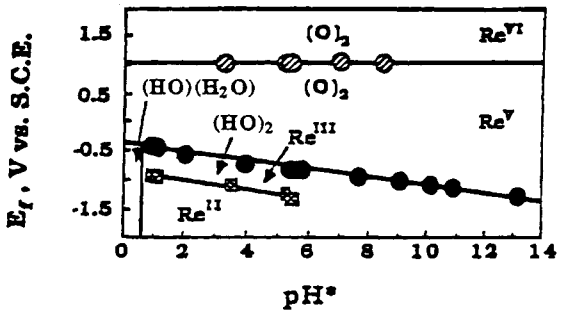

Figure 6. Pourbaix diagram for *t*-$(O)_2Re(MeOpy)_4^+$ in 50:50 CH_3CN/water.

$$(O)(MeO)Re^{V}L_4^{2+} + 2e^- + H^+ \rightarrow (HO)(MeO)Re^{III}L_4^+ \quad (9)$$

mentioning. First, oxo methylation shifts the Re(V/III) formal potential positive by roughly 200 mV (at pH* = 8). Secondly, the electrochemical kinetics (as measured by voltammetry peak separations) are substantially accelerated by methylation.

Returning to the first point, the observed thermodynamic differences between related $(O)(MeO)ReL_4^{2+}$ and $(O)_2ReL_4^+$ reductions are significantly dependent upon the pH* at which the observations are made. Figures 6 and 7 (middle) present plots of E_f versus pH* ("Pourbaix plots") for the pair of complexes, *t*-$(O)_2Re(MeOpy)_4^+$ and *t*-$(O)(MeO)Re(MeOpy)_4^{2+}$. Over most of the available pH* range, the dioxorhenium(V) reduction proceeds by the two-electron, two-proton reaction of eq 1.[28] (The proton stoichiometries (p) for the redox reactions have been determined from the slopes of the Pourbaix plots (ca. 60 mV in each case), where the slopes more generally will equal −59 (p/n) mV per pH* unit.) Below pH* = 6, further reduction to Re(II) is detectable:[8]

$$(HO)_2Re^{III}L_4^+ + e^- + H^+ \rightarrow (H_2O)(HO)Re^{II}L_4^+ \quad (10)$$

The oxo, methoxo complex differs from the dioxo complex in that (a) the Re(III/II) couple is not observed within the accessible solvent stability window (it is observed with other complexes), (b) the Re(V/III) couple is accompanied by only a single proton transfer (eq 11), and (c) at pH*'s above ap-

$$(O)(MeO)Re^{V}L_4^{2+} + 2e^- + H^+ \rightarrow (HO)(MeO)Re^{III}L_4^+ \quad (11)$$

proximately 10, the V/III reaction separates into its component steps and the elusive Re(IV) state appears. The portion of the Pourbaix plot above pH* ≈ 10 shows that the one-electron reduction reactions are:

$$(O)(MeO)Re^{V}L_4^{2+} + e^- \rightarrow (O)(MeO)Re^{IV}L_4^+ \quad (12)$$

and

$$(O)(MeO)Re^{IV}L_4^+ + e^- + H^+ \rightarrow (HO)(MeO)Re^{III}L_4^+ \quad (13)$$

Extension of the studies to four of the five other $(O)(MeO)Re^{V}L_4^{2+}$ complexes has yielded the Pourbaix data shown in Figures 7 (top and bottom) and 8. Additional dioxo results (previously unpublished) are shown in Figure 9. As one might expect, the general reactivity pattern is similar to that illustrated above. An instructive trend, however, is a shift in the Re(V/IV)/Re(IV/III) separation point toward higher pH* values as the electron-donating strength of the pyridyl ligand substituents is increased. Indeed, for the two most strongly donating substituents (dimethylamine and pyrrolidine, Figure 8), the separation point is shifted out of the available pH* range (i.e., resolution of the single-electron reduction components is never seen). Comparison of the single-electron potentials for the other four complexes (Figures 7 and 8, Table 5) gives some insight: For the proton-*de*coupled Re(V/IV) reaction, the formal potential moves to more negative values as the substituent electron-donating strength is increased. This is consistent, of course, with the usual differential stabilization of the higher oxidation state by ligand electron-donation effects. For the Re(IV/III) couple, on the other hand, there is almost no dependence of E_f on ancillary ligand identity. It is tempting, on the basis of our own previous work, to interpret the behavior in terms of "electron/proton compensation effects", i.e., offsetting effects due to simultaneous hydroxo ligand pK_a shifts and isolated electron-transfer potential shifts.[4c] Results presented in the next

(28) Below pH* ≈ 0 the reactant is $(O)(HO)Re^{V}(Mepy)_4^{2+}$.

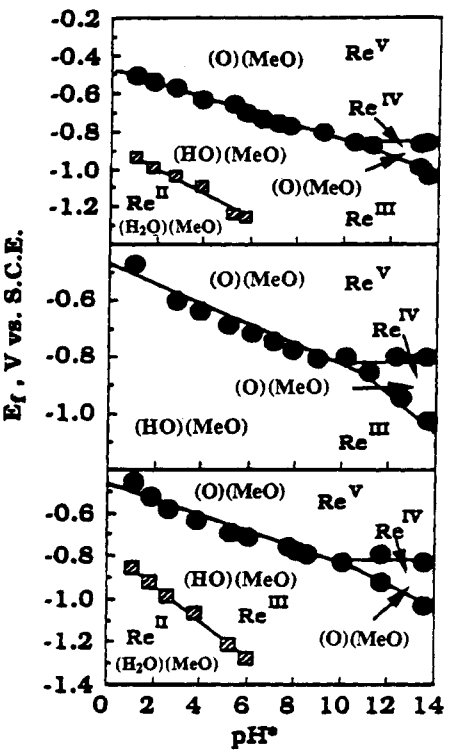

Figure 7. Pourbaix diagrams for *t*-$(O)(MeO)Re(py)_2(dmap)_2^{2+}$ (top), *t*-$(O)(MeO)Re(MeOpy)_4^{2+}$ (middle), and *t*-$(O)(MeO)Re(Me_2py)_4^{2+}$ (bottom) in 50:50 CH_3CN/water.

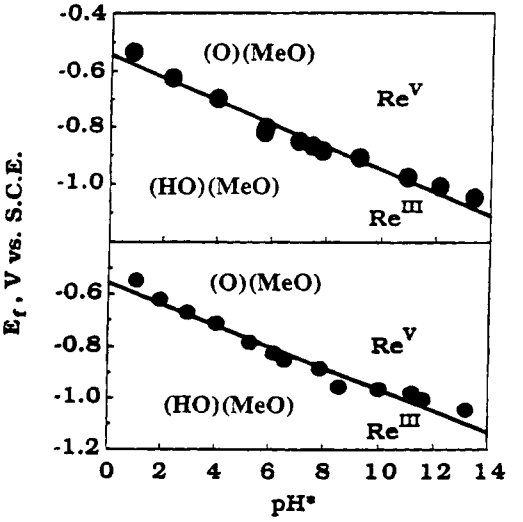

Figure 8. Pourbaix diagrams for *t*-$(O)(MeO)Re(pyrrpy)_4^{2+}$ (top) and *t*-$(O)(MeO)Re(dmap)_4^{2+}$ (bottom) in 50:50 CH_3CN/water.

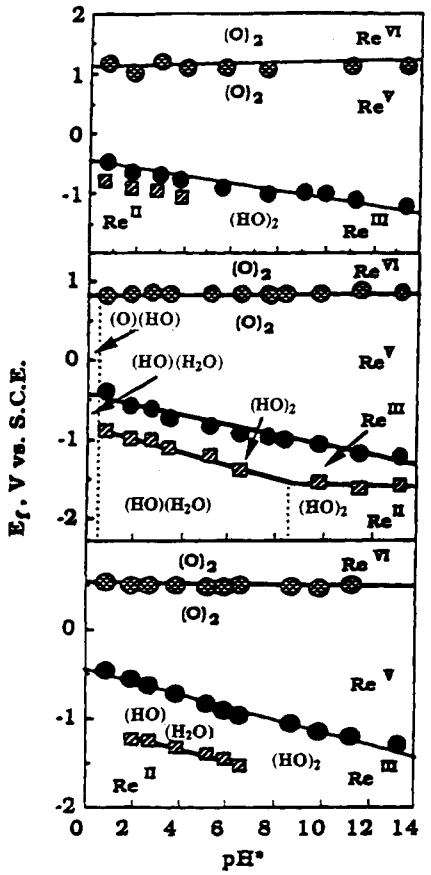

Figure 9. Pourbaix diagrams for t-$(O)_2Re(Me_2py)_4^+$ (top), t-$(O)_2Re(py)_2(dmap)_2^+$ (middle), and t-$(O)_2Re(pyrrpy)_4^+$ (bottom) in 50:50 CH_3CN/water.

Table 5. Aqueous Redox Potentials (pH* = 7.8) for t-$(O)(OMe)ReL_4^{2+}$ and t-$(O)_2ReL_4^+$ Complexes

complex	E_f(V/III)[a,b]
$(O)(MeO)Re(4\text{-}pyrrpy)_4^{m+}$	−0.87
$(O)_2Re(pyrrpy)_4^{n+}$	−1.00[c]
$(O)(MeO)Re(dmap)_4^{m+}$	−0.86
$(O)_2Re(dmap)_4^{n+}$	−1.03[c]
$(O)(MeO)Re(py)_2(dmap)_2^{m+}$	−0.76
$(O)_2Re(py)_2(dmap)_2^{n+}$	−0.97[c]
$(O)(MeO)Re(MeOpy)_4^{m+}$	−0.73
$(O)_2Re(MeOpy)_4^{n+}$	−0.97[c]
$(O)(MeO)Re(Me_2py)_4^{m+}$	−0.72
$(O)_2Re(Me_2py)_4^{n+}$	−0.96[c]
$(O)(MeO)Re(Mepy)_4^{m+}$	−0.71
$(O)_2Re(Mepy)_4^{n+}$	−0.96[c]

[a] Formal potentials in 50:50 CH_3CN/H_2O buffered at pH* = 7.8. [b] In volts vs SSCE. [c] Data taken from ref 4c.

section, however, show that E_f(IV/III) is ligand insensitive (or nearly so) even when proton uptake is decoupled from the reduction reaction. In any case, the observation of understandable trends in the separated V/IV and IV/III potentials permits one to make reasonable guesses for the potentials in the two instances where separation is not seen.

Finally, attempts instead to *oxidize* the $(O)(MeO)Re^VL_4^{2+}$ species were frustrated by the onset of water oxidation at far positive potentials (however, see next section).

Electrochemistry: Nonaqueous Experiments. In an effort both to access the Re(VI/V) couple and to disconnect the Re(V) and Re(IV) reductions from proton uptake, a series of electrochemical measurements was made in dry acetonitrile. A

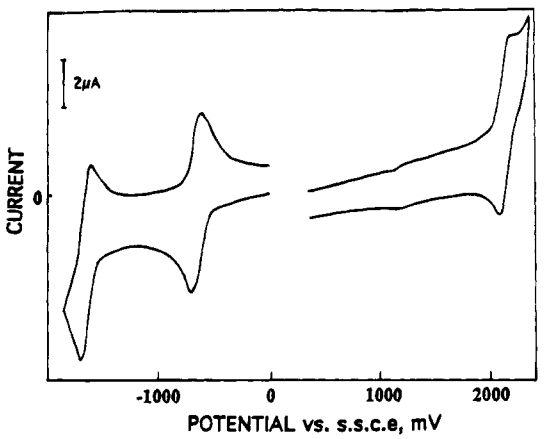

Figure 10. Cyclic voltammogram (sweep rate = 1 V/s) for t-$(O)(MeO)Re(Mepy)_4^{2+}$ in acetonitrile with 0.1 M $TBAPF_6$ as electrolyte.

Table 6. Nonaqueous Redox Potentials for $(O)(MeO)ReL_4^{m+}$ and t-$(O)_2ReL_4^{n+}$ Complexes

complex	E_f(VI/V)[a,b]	E_f(V/IV)[a,b]	E_f(IV/III)[a,b]
$(O)(MeO)Re(4\text{-}pyrrpy)_4^{m+}$	1.30	−1.08	−1.75
$(O)_2Re(pyrrpy)_4^{n+}$	0.55		
$(O)(MeO)Re(dmap)_4^{m+}$	1.39	−1.08	−1.83
$(O)_2Re(dmap)_4^{n+}$	0.53		
$(O)(MeO)Re(py)_2(dmap)_2^{m+}$	1.61	−0.86	−1.72
$(O)_2Re(py)_2(dmap)_2^{n+}$	0.86		
$(O)(MeO)Re(MeOpy)_4^{m+}$	1.98	−0.81	−1.78
$(O)_2Re(MeOpy)_4^{n+}$	1.04		
$(O)(MeO)Re(Me_2py)_4^{m+}$	2.12	−0.77	−1.60
$(O)_2Re(Me_2py)_4^{n+}$	1.17		
$(O)(MeO)Re(Mepy)_4^{m+}$	2.20	−0.74	−1.60
$(O)_2Re(Mepy)_4^{n+}$	1.12		

[a] Formal potentials in acetonitrile with 0.1 M $TBAPF_6$ electrolyte. [b] In volts vs. SSCE.

cyclic voltammogram for a representative compound, $(O)(MeO)Re(MeOpy)_4^+$, is shown in Figure 10. Key features are a reversible one-electron oxidation (to Re(VI)) at +1.98 V (eq 14) and consecutive, reversible[29] one-electron reductions at

$$t\text{-}(O)(MeO)Re^{VI}L_4^{3+} + e^- \rightarrow t\text{-}(O)(MeO)Re^{V}L_4^{2+} \quad (14)$$

−0.81 and −1.78 V (eqs 12 and 15). (Note that reaction 12

$$t\text{-}(O)(MeO)Re^{IV}L_4^{+} + e^- \rightarrow t\text{-}(O)(MeO)Re^{III}L_4^{0} \quad (15)$$

occurs at −0.81 V in 50:50 CH_3CN/H_2O as well; see above.) Attempts to extend the measurements to dioxo compounds yielded well-defined Re(V) oxidations (see Table 6), but ill-defined reductions.[30] In any case, generalized comparisons show (1) that methylation substantially increases E_f(VI/V) and (2) that elimination of proton transfer substantially destabilizes the lowest oxidation states, thereby fully separating the V/IV and IV/III redox steps.

Extension of the electrochemical measurements to other oxo, methoxo compounds (Table 6) shows that an enormous sensitiv-

(29) In the majority of cases involving other $(O)(MeO)ReL_4$ species, the IV/III step was only quasi-reversible in an electrochemical kinetic sense (e.g., peak seaprations of ca. 200 mV at a sweep rate of 0.1 V/s). Apparently this reduction entails somewhat larger internal mode displacements (activation barrier requirements) than do the VI → V and V → IV reductions. Reasonably accurate E_f values were still obtainable, however, by making measurements at very slow sweep rates.

(30) It is conceivable, based on the oxo, methoxo results, that the proton-decoupled dioxorhenium(V/IV) formal potential lies negative of the (presumably) irreversible reduction potential of ligated pyridine derivatives.

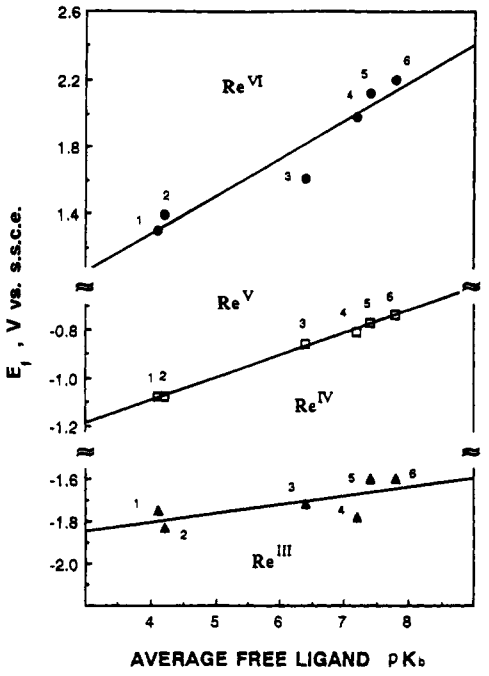

Figure 11. Formal potentials in acetonitrile for *t*-(O)(MeO)$ReL_4^{3+/2+/1+/0}$ vs free ligand (L) basicity. Key to ligands: (1) pyrrpy, (2) dmap, (3) py + dmap, (4) MeOpy, (5) Me_2py, (6) Me-py.

ity to ancillary (i.e., pyridyl) ligand composition exists for E_f(VI/V). Figure 11 shows more clearly that the E_f variations are related to pyridyl ligand basicity (or equivalently, substituent electron-donating strength). For E_f(V/IV), the dependence on basicity is diminished by roughly 2-fold, while for the IV/III reaction it is nearly absent (see Table 6 and Figure 10). The enhanced sensitivity of E_f(VI/V) can presumably be understood in terms of simple d-orbital occupancy effects. The electronic configuration of Re(V) is d^2, with both electrons confined to d_{xy}, i.e., the one d orbital coincident with the tetrapyridylrhenium plane. The energetics of conversion to d^1 should be exceptionally sensitive, therefore, to any factors influencing pyridyl nitrogen electron density.[5f] On the other hand, conversion to d^3 or d^4 (with occupancy of d_{xz} and/or d_{yz}) should be less strongly influenced. Still unclear, however, is why the d^2/d^3 and d^3/d^4 couples should differ so greatly in their response to substituent effects.

Discussion

The synthetic observations are clearly consistent with a simple electrophilic attack upon one of the two available, formally dinegative, oxo ligands as the mechanism for oxo, methoxo complex formation. Coordination to rhenium(V), of course, greatly diminishes the effective charges (and therefore the reactivity) at the oxo sites. (It also greatly diminishes the reactivity of tertiary amine substituents.) The residual oxo charge density (and reactivity) evidently can be significantly manipulated by manipulating the ancillary ligand identity. Indeed, the reactivity/residual-oxo-charge correlation is nicely illustrated, in a qualitative way, by the variation of reaction yield (see Experimental Section) with the corresponding *t*-(O)(HO)-$Re^VL_4^{2+}$ pK_a (i.e., higher yields with higher pK_a's). The pK_a analogy is also instructive with regard to geometric effects; the cis complexes, which resist methylation, also show no propensity (in oxidation state V) toward protonation.[4b]

Carrying the protonation analogy further, the general absence of double protonation of the trans complexes in oxidation state V (even at extreme pH's) is paralleled synthetically by the absence of dimethoxo products. Inactivation following the initial methylation is a finding consistent with the available X-ray and Raman data for *t*-(O)(MeO)ReL_4^{2+} (above). These show that the second rhenium−oxygen bond acquires substantial triple bond character. Presumably the increase in bond order is accompanied by further diminution in ligand charge density, thereby transforming the oxo into an extremely poor target for electrophilic (i.e., CH_3^+) attack.

Perhaps more surprising than the formation of the rhenium alkoxides[31] is the persistence of these high-oxidation-state species through workup in aqueous solution and subsequent characterization in both strongly acidic and strongly basic aqueous environments. Evidently, the rhenium−methoxo and the oxo−methyl linkages are very much less polar (less ionic), and more covalent, than the formal oxidation states would suggest.

Aqueous Electrochemistry. Clearly the most interesting and important electrochemical observation, from a mechanistic kinetics viewpoint, is the appearance of the key intermediate state, Re(IV), for several of the oxo, methoxo complexes at high pH*'s. To place this finding in perspective, however, it is necessary to consider first the redox behavior at lower pH*'s. Here the Pourbaix slopes are ca. 30 mV and 60 mV per pH* unit for the two-electron reductions of the oxo, methoxo- and dioxorhenium(V) complexes,[4a,c] respectively. The slope difference indicates that not only are the two sets of V/III formal potentials pH* dependent, but also their *differences* are pH* dependent. For example, the initially quite disparate (high pH*) potentials for (O)(MeO)$Re(Me_2py)_4^{2+}$ and $(O)_2Re(Me_2py)_4^+$ reduction (see Figures 7 and 9) eventually converge near pH* = 0. Importantly, this pH* value is essentially the value at which the dioxorhenium(V) compound becomes protonated and the reduction becomes a two-electron, one-proton process (eq 16). (The same is true for other oxo, methoxo/dioxorhenium

$$t\text{-(O)(HO)}Re^{V}L_4^{2+} + 2e^- + H^+ \rightarrow t\text{-(HO)}_2Re^{III}L_4^+ \quad (16)$$

pairs). It follows then, that reactions 11 and 16 have essentially identical thermodynamics, a result consistent with the nearly identical spectroscopic properties of (O)(MeO)ReL_4^{2+} and (O)-(HO)ReL_4^{2+} species.

In view of both the redox energetics and the spectroscopy, we conclude that the methoxo ligand and complex can be viewed as essentially the equivalent of the hydroxo ligand and complex, with one important difference: the methyl cation (unlike the proton) is irreversibly bound.

This interpretation (or conclusion) has a number of interesting consequences. First, the substantial difference in oxo-, methoxorhenium(V→III) versus dioxorhenium(V→III) electrochemical kinetics (Figure 5) can be taken as a direct measure of the kinetic cost of preequilibrium protonation (eq 2) in the overall multi-electron, multi-proton sequence (Scheme 1) for $(O)_2Re^VL_4^+$ reduction. A second point is that the (O)(MeO)-ReL_4^+ species can be used to project *what would have occurred* energetically at higher pH*'s in the (O)(HO)$Re^VL_4^+$ reduction reaction, if the hydroxyl proton had not dissociated. The most obvious result is that for four of the six complexes the Re(V/IV) and Re(IV/III) processes would have separated. The availability of separate one-electron (or one-electron, one-proton) potentials is highly significant because it ultimately provides a basis for understanding the kinetically relevant stepwise energetics of the multi-ET processes. For example, from Figures 7

(31) Oxo, *phen*oxides of rhenium(V) have also been prepared (by using benzyl bromide as an aryl cation source). These species are similar, both electrochemically and spectroscopically, to the oxo, methoxo complexes described here. (Ram, M. S. Unpublished results.)

Table 7. Estimated pK_a Values for $(O)(HO)Re^{VI}L_4^{3+}$ Complexes

complex	pK_a(VI)[a]
$(O)(HO)Re(pyrrpyr)_4^{3+}$	−10.4[b]
$(O)(HO)Re(dmap)_4^{3+}$	−12.3[c]
$(O)(HO)Re(py)_2(dmap)_2^{3+}$	−12[c]
$(O)(HO)Re(MeOpy)^{3+}$	−15.4[c]
$(O)(HO)Re(Me_2py)_4^{3+}$	−16[d]
$(O)(HO)Re(Mepy)_4^{3+}$	−18[d]

[a] Estimated via eq 17; see text. [b] Required pK_a for $(O)(HO)Re^{V}(pyrrpyr)_4^{2+}$ assumed to equal that for $(O)(HO)Re^{V}(dmap)_4^{2+}$. [c] Required p$K_a$ for $(O)(HO)Re^{V}L_4^{2+}$ taken from ref 4c. [d] Required pK_a for $(O)(HO)Re^{V}L_4^{2+}$ estimated on the basis of pyridyl (free ligand)/hydroxo (bound ligand) acidity correlation reported in ref 4c.

and 8 and related data for $(O)_2ReL_4^+$ species, one should be able to determine whether electrochemical reaction rates measured at the two-electron reduction potential are actually occurring at a significant overpotential or at an underpotential with respect to the energetics of the rate-determining step. We intend to report elsewhere on detailed interpretations of multi-ET kinetics, using the stepwise thermodynamics. To make the point here, however, it may be sufficient to recognize that (1) the observed V/III potentials are simply arithmetic means of V/IV and IV/III potentials, and (2) the latter can be obtained in a straightforward fashion at lower pH*'s by extrapolation from higher pH*'s.

Nonaqueous Electrochemistry. Like the high pH* aqueous measurements, the E_f measurements in dry acetonitrile provide effective access to the isolated thermodynamics of reaction 3 (i.e., the rate-determining step in the overall two-electron, two-proton reduction of dioxorhenium(V)). The isolated thermodynamics of an alternative rate-determining step,[15] reaction 4, are provided (approximately) by the E_f for reaction 15. When combined with the available data for the preequilibrium protonation of Re(V) (eq 2, Table 7), these measurements then permit the kinetically relevant multi-ET reaction energetics, up through transition-state precursor formation (i.e., either $(O)(HO)Re^{V}L_4^+$ or $(O)(HO)Re^{IV}L_4^0$), to be determined. Indeed, we are currently exploiting this information in the analysis of measured, pH-dependent, reaction kinetics.[32] In addition, $(O)(MeO)ReL_4^{n+}$ redox measurements in nonaqueous media, especially when combined with aqueous $(O)_2ReL_4^+$ measurements, offer a unique method for assessing proton binding strengths over an exceptionally wide range of pK_a's. The key, as suggested above, is to treat CH_3^+ as a nonlabile surrogate for H^+, when bound to an oxo group. We then can gain effective energetic access to such unlikely species as $(O)(HO)Re^{VI}L_4^{3+}$. Knowledge of the pH-independent reduction potential (as represented by the oxo, methoxo complex) may then be exploited in conjunction with the pH-independent dioxorhenium(VI/V) potential to yield relative pK_a's for hydroxo ligands in the Re(VI) and Re(V) oxidation states:

$$E_f(\text{VI/V})(\text{oxo, methoxo}) - E_f(\text{VI/V})(\text{dioxo}) \approx RT/nF \ln [K_a(\text{VI})/K_a(\text{V})] \quad (17)$$

Equation 17 shows that for a one-electron reaction, the formal potentials for the two types of redox complexes will differ by 59 mV (for $n = 1$) for each factor of 10 difference in acid (hydroxo ligand) dissociation constants. For the complexes examined here, the oxidation-state-dependent pK_a's differ by 12 to 18 orders of magnitude (on the basis of potential differences of 750 to 1080 mV; see Table 6). pK_a's for most of the rhenium(V) species have been reported previously.[4c] These range from +2.3 to approximately 0. The corresponding

(32) Hupp, J. T.; Zhang, X. L. Work in progress (see also ref 4d).

Table 8. Estimated pK_a Values (First pK_a) for $(HO)_2Re^{III}L_4^+$ Species

complex	pK_a[a]
$(HO)_2Re^{III}(pyrrpy)_4^+$	24
$(HO)_2Re^{III}(dmap)_4^+$	26
$(HO)_2Re^{III}(py)_2(dmap)_2^+$	25
$(HO)_2Re^{III}(MeOpy)_4^+$	25
$(HO)_2Re^{III}(Me_2py)_4^+$	22
$(HO)_2Re^{III}(Mepy)_4^+$	23

[a] Estimated from oxo,methoxorhenium electrochemical data as described in text. [b] Pourbaix slope for reaction 19b (required for pK_a estimation) not directly measured for this complex, but assumed to equal to 59 mV per pH* unit.

oxo-, hydroxorhenium(VI) pK_a's (eq 18), therefore, are estimated

$$t\text{-}(O)(HO)Re^{VI}L_4^{3+} \xrightarrow{K_a(\text{VI})} t\text{-}(O)_2ReL_4^{2+} + H^+ \quad (18)$$

as −10 to −18! Furthermore, the most negative values (see Table 7) are associated (as one would expect) with the complexes containing the least strongly electron-donating pyridine substituents. Turning the analysis around, the extremely negative $(O)(HO)Re^{VI}L_4^{3+}$ pK_a's illustrate just how crucial ligand deprotonation is in the stabilization of the higher oxidation states of oxo/hydroxo/aquo complexes.

On the basis of eq 18, we additionally conclude that dioxorhenium(VI) complexes will almost certainly be *in*effective as redox catalysts. Although the range of available Re(VI/V) potentials is attractive from a thermodynamic standpoint (particularly for common organic oxidation targets such as alcohols and olefins), the remarkable lack of affinity of $(O)_2Re^{VI}L_4^{2+}$ for protons (together with the very limited capability of $(O)_2Re^{V}L_4^+$ to bind protons) would argue against the possibility of coupled proton transfer or even H-atom extraction mechanisms for catalytic oxidation. Instead, it would appear that dioxorhenium(VI) species are capable of functioning only as simple redox mediators (i.e., single electron transfer agents) toward most oxidation targets.

Returning to thermodynamics, the combined aqueous and nonaqueous redox data can also be used to estimate the first pK_a for $(HO)_2Re^{III}L_4^+$:

$$t\text{-}(HO)_2Re^{III}L_4^+ \xrightarrow{K_a(\text{III})} t\text{-}(O)(HO)Re^{III}L_4^0 + H^+ \quad (19a)$$

$$t\text{-}(HO)(MeO)_2Re^{III}L_4^+ \xrightarrow{K_a(\text{III})} t\text{-}(O)(MeO)Re^{III}L_4^0 + H^+ \quad (19b)$$

We assume again that methoxo species (i.e., $(O)(MeO)Re^{III}L_4^0$ and $(HO)(MeO)Re^{III}L_4^+$) can function as surrogates for hydroxo species. We then observe that eq 19 chemically links eq 20

$$t\text{-}(O)(HO)Re^{IV}L_4^+ + e^- + H^+ \rightarrow t\text{-}(HO)_2ReL_4^+ \quad (20)$$

(or equivalently, eq 13) (the pH*-dependent, aqueous reduction of Re^{IV}; Figures 6−8) with eq 14 (or 4) (the pH*-independent, nonaqueous reduction of Re^{IV}). Thus, the formal potentials for the aqueous and nonaqueous reactions should coincide at the pH* value where $(HO)(MeO)Re^{III}L_4^+$ deprotonates (i.e., eq 19). Extrapolation of the available Pourbaix plots yields pK_a values of ca. +22 to +26 (see Table 8).

In principle, one should be able to use the remaining nonaqueous data to estimate pK_a's in other oxidation states. Unfortunately, the required auxiliary data for completion of the appropriate thermochemical cycles (e.g., pK_a for $(HO)(MeO)Re^{V}L_4^{3+}$, E_f for dioxorhenium(V/IV), etc.) are missing and

seemingly experimentally inaccessible. Some of these quantities would become accessible, however, if dimethoxo complexes (i.e., models for dihydroxo complexes) were available. As noted above, oxo, methoxorhenium(V) species resist further methylation. The corresponding Re(IV) species, on the other hand, might prove sufficiently electron rich to add a second methyl action. Presumably the needed reactants could be generated by controlled potential electrolysis of $(O)(MeO)Re^{V}L_4^{+}$ species in dry, oxygen-free organic solvents. We have not yet, however, explored this possibility experimentally.

Conclusions

High-valent, high-stability oxo-, methoxorhenium complexes can be prepared from the corresponding *trans*-dioxorhenium complexes and methyl trifluoromethanesulfonate. The new complexes behave nearly identically, in an electrochemical and spectroscopic sense, with the analogous oxo, hydroxo complexes, with one important exception: CH_3^{+}, unlike H^{+}, does not dissociate from the oxo ligand. The availability of a nonlabile proton analgoue permits one of the two usual proton-transfer steps to be disconnected from the usual two-electron reductions of rhenium(V) species. As a result, the ordinarily inaccessible Re(IV) state is stabilized relative to Re(III) and Re(V) and becomes electrochemically accessible at high pH*'s. The observation of the intermediate state is tremendously useful because it permits the stepwise thermodynamics of multi-electron, multi-proton transfer reactions to be mapped. This, in turn, is of central significance in corresponding kinetic studies. Additionally, the oxo-, methoxorhenium species can be used to obtain approximate thermodynamic information (acid dissociation constants) for ordinarily inaccessible complexes of the type $(O)(HO)Re^{VI}L_4^{3+}$, as well as for $(HO)_2Re^{III}L_4^{+}$ complexes.

Acknowledgments. We thank the Office of Naval Research and the DOD-AASERT program for support of this work. J.T.H. additionally acknowledges unrestricted support from the Dreyfus Foundation (Teacher-Scholar Award, 1991−96).

Supplementary Material Available: Tables of positional parameters, thermal parameters, interatomic distances, bond angles, and structure report and ORTEP for $[(O)(MeO)Re(py)_2(dmap)_2](PF_6)_2$ (15 pages); listing of structure factors (24 pages). This material is contained in many libraries on microfiche, immediately follows this article in the microfilm version of the journal, and can be ordered from the ACS; see any current masthead page for ordering information.

JA932581G